Original Article

The highly expressed *GOLPH3* in colorectal cancer cells activates smoothened to drive glycolysis and promote cancer cell growth and radiotherapy resistance

Kunli Zhu[1,2], Jing Fan[2], Hongchao Cai[3], Changchun Zhou[4], Zhe Gong[2], Zhenxiang Li[2]^, Jinming Yu[1,2]

[1]Shandong University Cancer Center, Shandong University, Jinan, China; [2]Department of Radiation Oncology, Shandong Cancer Hospital & Institute Affiliated to Shandong First Medical University, Shandong Academy of Medical Sciences, Jinan, China; [3]Department of Oncology, The First Affiliated Hospital of Shandong First Medical University & Shandong Provincial Qianfoshan Hospital, Jinan, China; [4]Department of Shandong Provincial Key Laboratory of Precision Oncology, Shandong Cancer Hospital &Institute Affiliated to Shandong First Medical University, Shandong Academy of Medical Sciences, Jinan, China

Contributions: (I) Conception and design: K Zhu; (II) Administrative support: K Zhu; (III) Provision of study materials or patients: Z Li, J Yu; (IV) Collection and assembly of data: K Zhu, J Fan, H Cai, C Zhou; (V) Data analysis and interpretation: Z Gong, Z Li, J Yu; (VI) Manuscript writing: All authors; (VII) Final approval of manuscript: All authors.

Correspondence to: Zhenxiang Li, PhD. Department of Radiation Oncology, Shandong Cancer Hospital & Institute Affiliated to Shandong First Medical University, Shandong Academy of Medical Sciences, Jiyan Road 440, Jinan 250117, China. Email: lizx0108@163.com; Jinming Yu, PhD. Shandong University Cancer Center, Shandong University, Jinan 250012, China; Department of Radiation Oncology, Shandong Cancer Hospital & Institute Affiliated to Shandong First Medical University, Shandong Academy of Medical Sciences, Jiyan Road 440, Jinan 250117, China. Email: sdyujinming@163.com.

Background: Colorectal cancer (CRC) is a frequently diagnosed cancer across the world and has increased in prevalence over the last decade. This study aimed to assess the biological roles, influences on radiosensitivity, and possible molecular mechanism of Golgi phosphoprotein 3 (*GOLPH3*) in CRC.

Methods: Western blotting, quantitative real-time polymerase chain reaction (qRT-PCR), and immunohistochemistry (IHC) were used to examine GOLPH3 expression. *In vivo* and *in vitro* assays were carried out to clarify the function of *GOLPH3* in CRC. The differentially expressed genes (DEGs) in CRC cells with knockdown of *GOLPH3* were identified through RNA sequencing (RNA-seq). Based on the DEGs associated with *GOLPH3* knockdown and the data from The Cancer Genome Atlas (TCGA) database, the pathways that could be regulated by *GOLPH3* were predicted via Kyoto Encyclopedia of Genes and Genomes (KEGG) enrichment analysis.

Results: In CRC, *GOLPH3* was upregulated, and *GOLPH3* upregulation was predictive of a poor prognosis. *GOLPH3* knockdown inhibited CRC cell proliferation, migration, and invasion but promoted apoptosis and reduced radiotherapy resistance. Conversely, in CRC cells with *GOLPH3* overexpression, malignant biological behavior and radiotherapy resistance were enhanced. *In vivo*, *GOLPH3* knockdown impeded tumor growth. Mechanistically, *GOLPH3* promoted the localization of smoothened (SMO) on the cell membrane, thereby activating AMP-activated protein kinase (AMPK)-mediated glycolysis. Additionally, the final product of glycolysis, lactate, induced H3 lysine 18 lactylation (H3K18), which could be enriched on the promoter of *GOLPH3* and stimulate the transcription of *GOLPH3*.

Conclusions: *GOLPH3* promoted CRC progression and enhanced radiotherapy resistance via glycolysis mediated by the SMO-AMPK axis.

Keywords: Colorectal cancer (CRC); Golgi phosphoprotein 3 (GOLPH3); radiotherapy resistance; glycolysis

Submitted Mar 12, 2025. Accepted for publication Apr 21, 2025. Published online Apr 27, 2025.
doi: 10.21037/jgo-2025-193
View this article at: https://dx.doi.org/10.21037/jgo-2025-193

^ ORCID: 0000-0002-9648-8869.

© AME Publishing Company.

Introduction

As a frequently diagnosed cancer, colorectal cancer (CRC) accounted for approximately 550,000 new cancer cases and 286,000 deaths in China in 2020 (1). Over the past decade, CRC prevalence has declined in industrialized nations but has risen in China (2). In patients with CRC, the primary causes of treatment failure and death are distant metastasis and recurrence (1,3). Most patients with late-stage CRC are defined as initially unresectable, and the 5-year overall survival (OS) rate of these patients is less than 20% (4-6). Despite the significant progress made in refining molecular and immunological methods, the prognosis and treatment of advanced CRC remain unsatisfactory (7,8). In recent years, the standard treatment for CRC, especially local advanced rectal cancer, has included neoadjuvant radiotherapy (7,9). However, in clinical practice, treatment failure often occurs due to original or gradually adaptive radiotherapy resistance (10,11). Therefore, clarifying the molecular mechanisms related to radioresistance is critical for improving the prognosis of patients with CRC.

Golgi phosphoprotein 3 (*GOLPH3*) is located on the opposite sides of the Golgi apparatus, and its role involves protein glycation, protein classification, vesicle transport, and maintenance of the Golgi banding structure (12-14). Recently, *GOLPH3* has been reported to affect the progression of various cancers. For example, in breast cancer (BC), *GOLPH3* expression has been shown to be upregulated and its high expression associated with the poor prognosis (15). In pancreatic ductal adenocarcinoma (PDAC), GOLPH3 interacts with stress-induced phosphoprotein 1 and regulates telomerase activity to upregulate cell cycle-related proteins and facilitate tumor cell growth (16). In non-small cell lung cancer, *GOLPH3* overexpression increases tumorigenicity and metastasis through activating Wnt/β-catenin pathway (17). In addition, *GOLPH3* knockdown sensitizes lung adenocarcinoma cells to X-ray irradiation (18). The interaction between GOLPH3 and myosin-18A causes Golgi dispersal, impairing Golgi trafficking to enable cell survival after DNA damage (18). Gao *et al.* found that *GOLPH3* promotes sorafenib resistance and angiogenesis in hepatocellular carcinoma (19). Yu *et al.* reported that oxaliplatin resistance of colon cancer cells could be reversed via the inhibition of *GOLPH3*, which may be related to the suppression of the phosphatidylinositol 3-kinase (PI3K)/AKT/mammalian target of the rapamycin (mTOR) pathway (20). However, whether *GOLPH3* is involved in the radiotherapy resistance of CRC cells has not yet been fully determined.

In this study, we assessed *GOLPH3* expression in terms of its prognostic value for CRC. Next, we examined the biological and radiosensitivity regulating effects of *GOLPH3* on CRC cells by performing *in vitro* experiments. To further clarify the molecular mechanisms underlying *GOLPH3*'s role in CRC, Kyoto Encyclopedia of Genes and Genomes (KEGG) enrichment analysis was performed based on the data from RNA sequencing (RNA-seq) and The Cancer Genome Atlas (TCGA) database. Finally, *GOLPH3*'s roles and the related molecular mechanisms were confirmed *in vivo*. We present this article in accordance with the ARRIVE and MDAR reporting checklists (available at https://jgo.amegroups.com/article/view/10.21037/jgo-2025-193/rc).

Highlight box

Key findings

- Golgi phosphoprotein 3 (*GOLPH3*) promoted colorectal cancer (CRC) progression and enhanced radiotherapy resistance via glycolysis mediated by the smoothened (SMO)-AMP-activated protein kinase (AMPK) axis.

What is known and what is new?

- *GOLPH3* has been reported to affect the progression of various human cancers, including breast cancer, pancreatic ductal adenocarcinoma, non-small cell lung cancer, and hepatocellular carcinoma.
- Our study is the first of its kind to demonstrate the role of *GOLPH3* in the radiotherapy resistance of CRC cells and to clarify the related molecular mechanisms.

What is the implication, and what should change now?

- Our findings indicated that *GOLPH3* is a key regulator in CRC progression and the development of radiotherapy resistance. One of the mechanisms of the tumor-promoting effects of *GOLPH3* might be its regulation of glycolysis as mediated by SMO-AMPK signaling. Further study based on clinic data are required to confirm the potential of *GOLPH3* for use as a treatment target.

Methods

Bioinformatics analysis

The messenger RNA (mRNA) expression data and related clinical data of CRC in TCGA were obtained from the UCSC Xena database (http://xena.ucsc.edu/). Differential expression analysis was performed using the R package "DESeq2" version 1.44.0 (The R Foundation of Statistical Computing, Vienna, Austria). The R package "clusterProfiler" version 4.12.2 was used for KEGG enrichment analysis. The graphical visualization was

© AME Publishing Company.

implemented via the R package "ggplot2" version 3.5.1. All statistical analyses were conducted using R software version 4.4.1. Statistical significance was defined as a P value less than 0.05. The differences between the two groups were compared using the Wilcoxon test. Survival analysis was performed through the Kaplan-Meier method. For correlation analysis, the Spearman correlation coefficient was calculated.

Human specimens

This study was conducted in accordance with the Declaration of Helsinki and its subsequent amendments. The study was approved by the Ethics Committee of Shandong Cancer Hospital & Institute Affiliated to Shandong First Medical University (No. SDTHEC 2023006022) and informed consent was taken from all the patients. CRC tissue and adjacent tissue from 41 patients were collected at Shandong Cancer Hospital & Institute Affiliated to Shandong First Medical University between July 2023 and June 2024. None of the patients underwent antitumor therapy, including immunotherapy, chemotherapy, targeted therapy, and surgery.

Cell culture

Human CRC cell lines (LoVo, SW480, HT-29, and HCT-116) were purchased from Nanjing Cobioer Biosciences Co., Ltd. (Nanjing, China). LoVo and SW480 cells were cultured in Dulbecco's Modified Eagle Medium (DMEM; Sigma-Aldrich, St. Lous, MO, USA). HT-29 and HCT-116 cells were cultured in Roswell Park Memorial Institute (RPMI) 1640 medium (Sigma-Aldrich) and McCoy's 5a medium (Sigma-Aldrich), respectively. All media were mixed with 10% fetal bovine serum (FBS; Sigma-Aldrich). At 37 ℃, all cells were grown in an incubator with a 5% CO_2 atmosphere.

Cell transfection

According to the manufacturer's instructions, transfection was carried with Lipofectamine 3000 (Invitrogen, Themo Fisher Scientific, Waltham, MA, USA). HCT-116 cells were transfected with *GOLPH3* overexpression vector (OE-GOLPH3) and negative control vector (OE-NC). SW480 cells were transfected with small interfering RNA (siRNA) targeting *GOLPH3* (si1-GOLPH3, 5'-GTGGCTGTATGTTAATTGAAT-3'; si2-GOLPH3, 5'-GCATTGAGAGGAAGGTTACAA-3') and scrambled siRNA (si-NC, 5'-GTGTTAAATCTAGTGTGAGTT-3'). OE-GOLPH3, OE-NC, si1-GOLPH3, si2-GOLPH3, and si-NC were synthesized by Shanghai GenePharma Co., Ltd. (Shanghai, China).

Radiosensitivity assay

HCT-116 and SW480 cells were subjected to different doses of X-ray (0, 2, 4, and 6 Gy) via a 6-MV linear accelerator (Elekta, Stockholm, Sweden). To assess *GOLPH3*'s effects on CRC radiotherapy resistance, HCT-116 and SW480 cells were subjected to ionizing radiation (IR) after transfection.

Quantitative real-time polymerase chain reaction (qRT-PCR)

Through TRIzol (Thermo Fisher Scientific, Waltham, MA, USA), RNA was extracted from tissues and cells. Next, complement DNA (cDNA) was generated with a PrimeScriptRT reagent kit (Takara Bio, Kusatsu, Japan). Power SYBR Green PCR master mix (Applied Biosystems, Thermo Fisher Scientific) was employed for performing qRT-PCR. The quantification of *GOLPH3* expression was calculated according to $2^{-\Delta\Delta CT}$ method. The primers' sequence information is as follows: *GOLPH3* forward, 5'-AAGGACCGCGAGGGTTACAC-3'; *GOLPH3* reverse, 5'-CGTCTCATTCCACAAGCCTCT-3'; glyceraldehyde-3-phosphate dehydrogenase (*GAPDH*) forward, 5'-GAATGGGCAGCCGTTAGGAA-3'; and *GAPDH* reverse, 5'-CCCAATACGACCAAATCAGAGA-3'.

Western blotting

Proteins in cells and tissues were extracted using RIPA lysis buffer (Beyotime Biotechnology, Nantong, China). After being subjected to sodium dodecyl sulfate-polyacrylamide gel electrophoresis (SDS-PAGE), proteins were transferred to polyvinylidene fluoride (PVDF) membranes (Thermo Fisher Scientific). The membrane was incubated at 4 ℃ with primary antibodies acquired from Proteintech [GOLPH3, 19112-1-AP; GAPDH, 10494-1-AP; B cell lymphoma-2 (Bcl-2), 12789-1-AP; BCL2-associated X (Bax), 50599-2-Ig; cleaved (C)-caspase-3, 82707-13-RR; E-cadherin, 20874-1-AP; N-cadherin, 22018-1-AP; Vimentin, 80232-1-RR; AMP-activated protein kinase (AMPK), 10929-2-AP; phosphorylated (p)-AMPK, 83924-1-RR; pyruvate kinase M2 (PKM2), 15822-1-AP; Histone

© AME Publishing Company.

H3, 17168-1-AP; Rosemont, IL, USA], PTM Biolabs [H3 lysine 18 lactylation (H3K18la), PTM-1406RM; Chicago, IL, USA], and Abcam (Snail, ab216347; Cambridge, UK) after being blocked with 5% nonfat milk. The next day, a secondary antibody (ab7090; Abcam) was used to incubate the membrane for 1 hours. After being visualized by an enhanced chemiluminescence (ECL) kit (Thermo Fisher Scientific), protein bands were gauged via ImageJ software (US National Institutes of Health, Bethesda, MD, USA).

Cell Counting Kit-8 assay (CCK-8)

After being seeded in 96-well plates, HCT-116 and SW480 cells were cultured for 12, 24, 48, and 72 hours, respectively. Subsequently, cells were exposed to CCK-8 reagents (Dojindo, Kumamoto, Japan). Two hours later, at a wavelength of 450 nm, the optical density (OD) was tested with a microplate reader (Thermo Fisher Scientific).

Colony formation

HCT-116 and SW480 cells were seeded in six-well plates. Two weeks later, cells were fixed and stained in 4% paraformaldehyde (PFA; Solarbio, Beijing, China) and crystal violet (Sigma-Aldrich), respectively. Finally, the number of colonies with more than 50 cells was counted.

5-Ethynyl-2-deoxyuridine (EdU) assay

HCT-116 and SW480 cells were inoculated in 24-well plates. After being exposed to EdU assay (RiboBio, Guangzhou, China) for 2 hours, cells were fixed by 4% PFA and then treated with 0.5% Triton X-100 (Sigma-Aldrich). Subsequently, cell nuclei were stained with 4',6-diamidino-2-phenylindole (DAPI; Beyotime Biotechnology). Under a fluorescence microscope (Olympus, Tokyo, Japan), we observed EdU-positive cells.

Flow cytometry

After indicated treatment, HCT-116 and SW480 cells were resuspended in Annexin V-FITC binding buffer (Beyotime Biotechnology). Annexin V-FITC and propidium iodide (PI) were used for incubating cells in the dark. Twenty minutes later, cell apoptosis was analyzed via flow cytometry (BD Biosciences, Franklin Lakes, NJ, USA).

Wound healing assay

HCT-116 and SW480 cells were inoculated into six-well plates and cultured in serum-free medium. A wound was created with a 200-μL sterile pipette tip when cell confluence reached 100%. Twenty-four hours later, the images of wound healing were recorded under a microscope (Leica, Wetzlar, Germany).

Transwell assay

HCT-116 and SW480 cell migration and invasion were assessed through the use of Transwell chambers (Costar-Corning, NY, USA). In brief, a serum-free cell suspension was added into the upper compartment of a migration (Matrigel-uncoated insert) or invasion (Matrigel-coated insert) chamber, and medium supplemented with 10% FBS was added into the lower chamber. After 24-hour culturing, the migrated and invaded cells were fixed and stained with 4% PFA and crystal violet, respectively. Finally, the number of migrated and invaded cells was recorded under a microscope.

Microarray analysis

RNA in SW480 cells with si-GOLPH3 or si-NC transfection was extracted for second-generation RNA-seq. Through TRIzol, total RNA was separated and purified. The amount and purity of total RNA were measured using the NanoDrop 1000 spectrophotometer (Thermo Fisher Scientific), and the integrity of RNA was tested with the Bioanalyzer 2100 (Agilent Technologies, Santa Clara, CA, USA). When the concentration was >50 ng/μL, RNA integrity number (RIN) value >7.0, and total RNA >1 μg, the subsequent experiments were performed. The mRNA with PolyA was specifically captured through two rounds of purification using oligo magnetic beads (Thermo Fisher Scientific). The obtained mRNA was fragmented using the NEBNextR Magnesium RNA Fragmentation Module (New England Biolabs, Ipswich, MA, USA) at 94 ℃ for 5–7 minutes. The fragmented RNA was synthesized into cDNA via SuperScript II Reverse Transcriptase (Invitrogen, Thermo Fisher Scientific). Next, *Escherichia coli* DNA polymerase I (New England Biolabs) and RNase H (New England Biolabs) were used for second strand synthesis, and then these complex double-strands of DNA and RNA were to converted into DNA double strands. Moreover, dUTP solution (Thermo Fisher Scientific) was incorporated into

© AME Publishing Company.

second strands. The blunt ends of double-stranded DNA were filled, and then an A base was added to each end to enable it to be connected to a linker with a T base at the end. The fragment size was screened and purified using magnetic beads. The second strand was digested with UDG enzyme (New England Biolabs), and then subjected to polymerase chain reaction (PCR) to form a library with a fragment size of 300±50 bp (strand-specific library). The PCR protocol was as follows: predenaturation at 95 ℃ for 3 minutes, denaturation at 98 ℃ for a total of 8 cycles of 15 seconds each, annealing at 60 ℃ for 15 seconds, extension at 72 ℃ for 30 seconds, and final extension at 72 ℃ for 5 minutes. Finally, we used the Novaseq^{TM} 6000 (Illumina, San Diego, CA, USA) under the PE150 sequencing mode to perform double-end sequencing.

Measurement of oxygen consumption rate (OCR) and extracellular acidification rate (ECAR)

The changes of ECAR and OCR in HCT-116 and SW480 cells were assessed with the Seahorse XFp Metabolic Analyzer (Agilent). In brief, cells (1×10^5 cells per well) were cultured in a Seahorse XFp cell culture plate (Agilent) overnight. Before OCR measurement for 1 hour in a CO_2-free incubator, cells were maintained in XF base medium containing 10-mM of glucose, 2-mM of glutamine, and 1-mM of pyruvate. Next, cells were incubated with 2-μM of oligomycin, 1-μM of carbonyl cyanide 4-(trifluoromethoxy) phenylhydrazone (FCCP), and 0.5 of μM rotenone and antimycin A. For ECAR measurement, cells were maintained in XF base medium containing 2-mM of glutamine for 1 hour. Next, the cells were incubated with 10-mM of glucose, 1-μM of oligomycin, and 50-mM of 2-deoxyglucose (2DG).

Measurement of glucose uptake

Glucose uptake was determined via a glucose uptake colorimetric assay kit (ab136955; Abcam). Briefly, after glucose starvation, HCT-116 and SW480 cells were exposed to 2DG for 20 minutes, washed with phosphate buffered saline (PBS), and then lysed with extraction buffer. The lysates were incubated with neutralizing buffer. After centrifugation, the supernatants were incubated with reaction mix A. One hour later, the samples were extracted and heated at 90 ℃ for 40 minutes. After being cooled on ice, the samples were incubated with reaction mix B. At 412 nm, the absorbance was recorded by a microplate reader.

Measurement of lactate level

The lactate level was determined with the L-Lactate Assay Kit (ab65331; Abcam). Briefly, after the indicated treatment, cell culture supernatants were collected and then added with reaction mix. Thirty minutes later, at 450 nm, the absorbance was recorded with a microplate reader.

Chromatin immunoprecipitation (ChIP) assay

The Pierce Magnetic ChIP Kit (Thermo Fisher Scientific) was employed for completing ChIP assay. In brief, cells were exposed to 1% formaldehyde (Sigma-Aldrich) and then sonicated to obtain DNA fragments. Next, DNA fragments were incubated with anti-IgG (30000-0-AP; Proteintech) or anti-H3K18la-ChIP grade (PTM-1427RM; PTM Biolabs) at 4 ℃. The next day, DNA-protein immunocomplexes were obtained with protein A/G magnetic beads. After being eluted and purified, DNA samples were subjected to PCR.

Xenograft mice model

Animal experiments were performed under a project license (No. SDTHEC 2023006021) granted by the Animal Ethics Committee of Shandong Cancer Hospital & Institute Affiliated to Shandong First Medical University, in compliance with the guidelines of Shandong Cancer Hospital & Institute Affiliated to Shandong First Medical University for the care and use of animals. A protocol was prepared before the study without registration. Mice (GemPharmatech, Nanjing, China) in the sh-NC group (n=5) and sh-GOLPH3 group (n=5) were subcutaneously injected with SW480 cells with sh-NC or sh-GOLPH3 transfection. The xenograft tumor volume was measured every 3 days from the 10th day of injection. At the 31st day of injection, all mice were euthanized, and tumors were removed to be weighed and subjected to immunohistochemistry (IHC), immunofluorescence (IF), terminal-deoxynucleoitidyl transferase mediated nick end labeling (TUNEL) assay, and Western blotting.

IHC analysis

Tissues were embedded in paraffin after being fixed in 4% PFA and dehydrated in gradient alcohol. After being cut, tissue sections were exposed to 3% H_2O_2 and then blocked through application of 4% normal goat serum (Invitrogen). Before being incubated with secondary antibody (ab7090),

© AME Publishing Company.

sections were incubated at 4 ℃ overnight with primary antibodies (GOLPH3, 19112-1-AP; H3K18la, PTM-1406RM; Ki67, 84432-1-RR; Proteintech). After being stained with DAB (Beyotime Biotechnology), sections were counterstained with hematoxylin (Beyotime Biotechnology). Finally, under a microscope, sections were examined.

TUNEL staining

The One Step TUNEL Apoptosis Assay Kit (Beyotime Biotechnology) was applied for detecting cell apoptosis. In brief, tissue sections were incubated for 20 minutes with protease K without DNase. After being washed with PBS, sections were exposed to TUNEL reaction mixture for 60 minutes in the dark. DAPI was applied for counterstaining sections. Under a fluorescence microscope, TUNEL positive cells were surveyed.

IF staining

For tissue, sections underwent antigen retrieval via application of sodium citrate buffer. For cells, HCT-116 and SW480 cells were fixed with 4% PFA and permeabilized in Triton X-100. Before being incubated with primary antibodies, including smoothened (SMO; 20787-1-AP; Proteintech), PKM2 (15822-1-AP; Proteintech), and H3K18la (PTM-1406RM; PTM Biolabs), sections or cells were incubated with goat serum for 1 h. subsequently, sections were incubated with secondary antibodies (ab150077 or ab150080; Abcam) and then stained with DAPI. Finally, SMO expression was analyzed under a fluorescence microscope.

Statistical analysis

Statistical analyses were conducted with GraphPad Prism software (Dotmatics, Boston, MA, USA). Experiments were repeated three times independently. All data are displayed as the mean ± standard deviation. A P value less than 0.05 indicated statistical significance. The statistical significance was determined via a Student's *t*-test and one-way analysis of variance (ANOVA).

Results

GOLPH3 expression was correlated with poor survival of patients with CRC

To investigate the correlation between *GOLPH3* expression and CRC progression, Kaplan-Meier survival analysis was performed based on the data from TCGA database. Superior survival was observed in patients with CRC with low *GOLPH3* expression (*Figure 1A*). Next, we assessed GOLPH3 expression in CRC tissues and their corresponding adjacent tissues. As displayed in *Figure 1B-1D*, GOLPH3 expression was markedly elevated in CRC tissues. Furthermore, GOLPH3 was overexpressed in CRC cell lines; and it was noticed that *GOLPH3* was highly expressed in SW480 cells while weakly expressed in HCT-116 cells (*Figure 1E*).

GOLPH3 promoted CRC cell proliferation and inhibited apoptosis

To further elucidate *GOLPH3*'s biological functions in CRC, GOLPH3 overexpression was induced in HCT-116 cells with lower GOLPH3 expression, and GOLPH3 was knocked down in SW480 cells with higher GOLPH3 expression (*Figure 2A*). As seen in *Figure 2B*, cell viability was promoted by *GOLPH3* overexpression and inhibited by *GOLPH3* knockdown. Additionally, *GOLPH3* overexpression facilitated cell proliferation, but cell proliferation was suppressed by *GOLPH3* knockdown (*Figure 2C,2D*). Flow cytometry revealed that cell apoptosis was reduced via *GOLPH3* overexpression and increased by *GOLPH3* knockdown (*Figure 2E*). Moreover, *GOLPH3* overexpression increased Bcl-2 expression and decreased Bax and C-caspase-3 expression, but GOLPH3 knockdown produced the opposite effect (*Figure 2F*).

GOLPH3 promoted CRC cell migration and invasion

Similar to cell proliferation and apoptosis, CRC cell migration and invasion were also influenced by *GOLPH3*. Cell migration and invasion were promoted by *GOLPH3* overexpression and inhibited by *GOLPH3* knockdown (*Figure 3A,3B*). Furthermore, *GOLPH3* overexpression in HCT-116 cells decreased E-cadherin expression and increased Snail, N-cadherin, and Vimentin expression, while the reverse was observed in SW480 cells with GOLPH3 knockdown (*Figure 3C*).

GOLPH3 promoted radiotherapy resistance of CRC cells

Next, we investigated *GOLPH3*'s change during radiotherapy for CRC. As shown in *Figure 4A*, X-rays increased *GOLPH3* expression in a dose-dependent manner. As indicated by CCK-8 assay, colony formation

© AME Publishing Company.

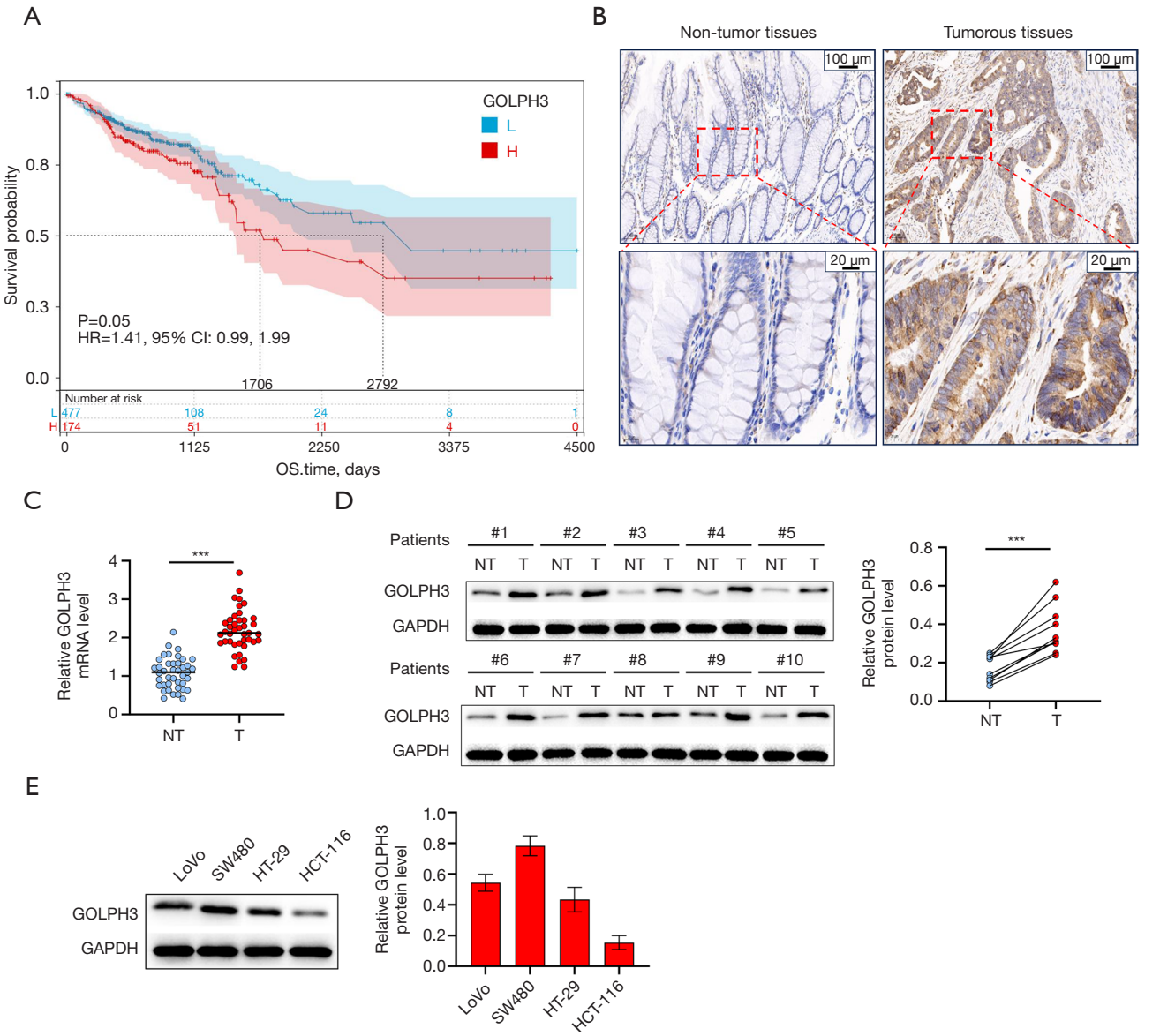

Figure 1 *GOLPH3* expression was correlated with poor survival in patients with CRC. (A) Based on TCGA database, the correlation between *GOLPH3* expression and survival of patients with CRC was assessed through Kaplan-Meier survival analysis. In CRC and normal tissues, GOLPH3 expression was examined via (B) IHC, (C) qRT-PCR, and (D) Western blotting. (E) GOLPH3 expression in CRC cell lines was analyzed via Western blotting. ***, P<0.001 *vs.* NT. GOLPH3, Golgi phosphoprotein 3; HR, hazard ratio; CI, confidence interval; L, low-expression; H, high-expression; OS, overall survival; NT, non-tumor; T, tumor; GAPDH, glyceraldehyde-3-phosphate dehydrogenase; CRC, colorectal cancer; TCGA, The Cancer Genome Atlas; IHC, immunohistochemistry; qRT-PCR, quantitative real-time polymerase chain reaction.

assay, and flow cytometry, *GOLPH3* overexpression promoted HCT-116 cell viability and proliferation and inhibited apoptosis under X-ray, but *GOLPH3* knockdown enhanced radiosensitivity in SW480 cells (*Figure 4B-4D*). In addition, *GOLPH3*'s effects on DNA double-strand breaks (DSBs) were detected. *GOLPH3* overexpression in HCT-116 cells reversed the increase of γ-H2AX induced by IR, while *GOLPH3* knockdown in SW480 cells

© AME Publishing Company.

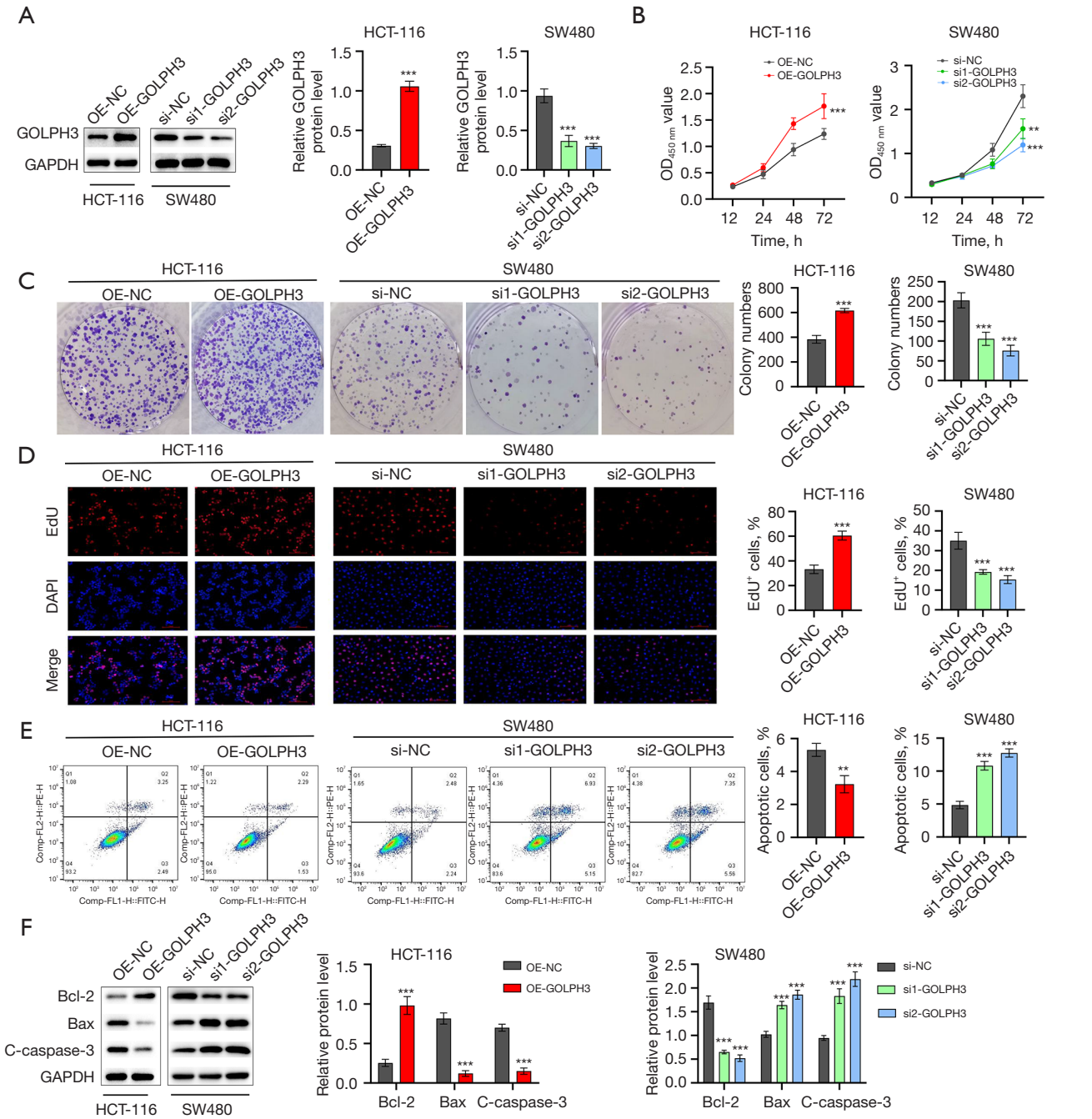

Figure 2 *GOLPH3* promoted CRC cell proliferation and inhibited apoptosis. (A) GOLPH3 expression in HCT-116 and SW480 cells was analyzed via Western blotting. (B) HCT-116 and SW480 cell viability was analyzed using CCK-8 assay. (C) Colony formation assay followed by crystal violet staining and (D) EdU staining were performed for assessing HCT-116 and SW480 cell proliferation. Scale bar =100 μM. (E) HCT-116 and SW480 cell apoptosis was analyzed via flow cytometry. (F) Bcl-2, Bax, and C-caspase-3 expression were checked by Western blotting in HCT-116 and SW480 cells. **, P<0.01, or ***, P<0.001 *vs.* si-NC or OE-NC group. GOLPH3, Golgi phosphoprotein 3; GAPDH, glyceraldehyde-3-phosphate dehydrogenase; Bcl-2, B cell lymphoma-2; Bax, BCL2-associated X; C-caspase-3, cleaved-caspase-3; OD, optical density; OE-NC, overexpression negative control; EdU, 5-ethynyl-2-deoxyuridine; DAPI, 4',6-diamidino-2-phenylindole; CRC, colorectal cancer; CCK-8, Cell Counting Kit-8.

© AME Publishing Company.

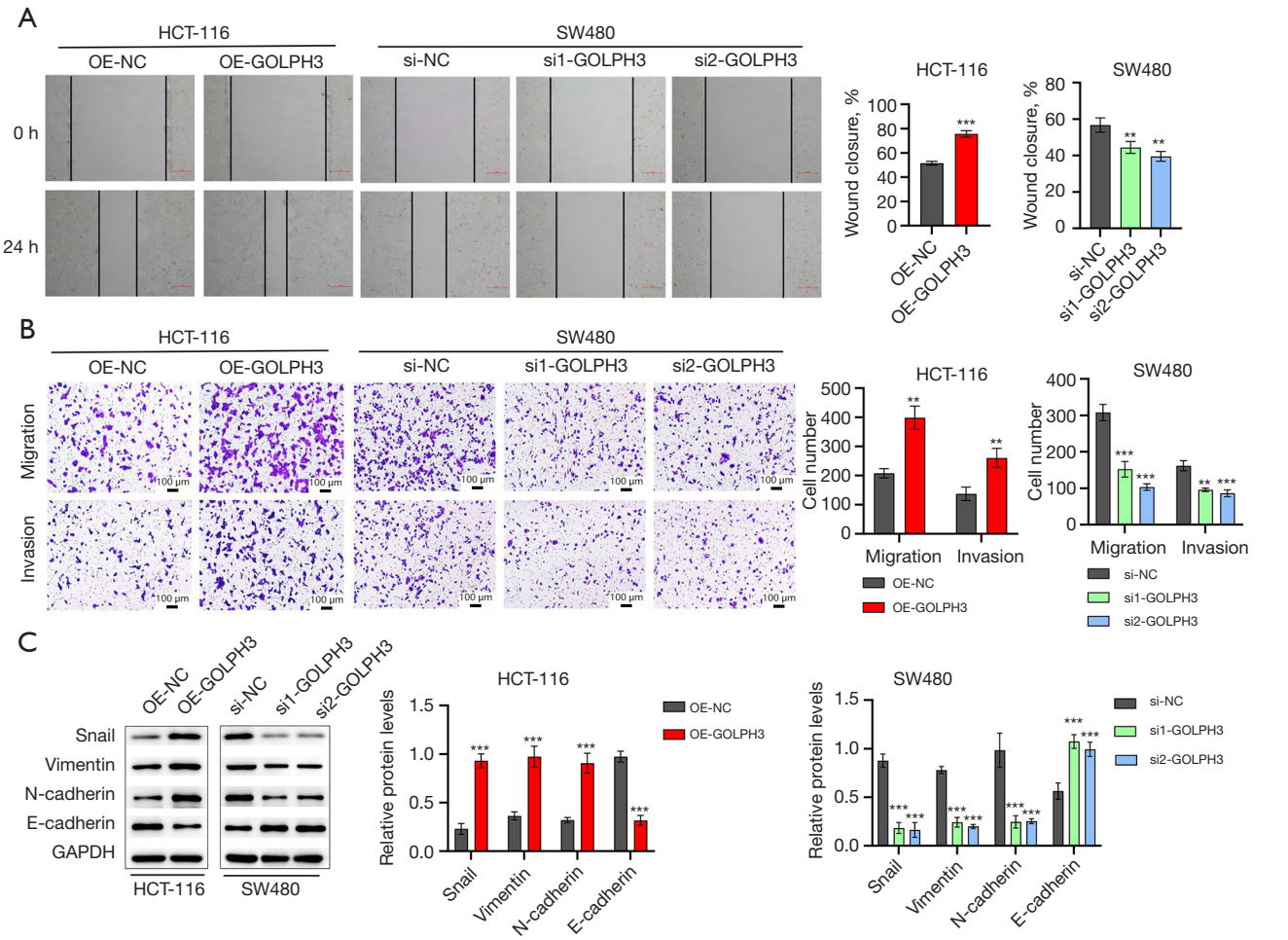

Figure 3 *GOLPH3* promoted CRC cell migration and invasion. (A) HCT-116 and SW480 cell migration were assessed via wound healing assay. Scale bar =500 μM. (B) HCT-116 and SW480 cell migration and invasion were assessed via Transwell assay followed by crystal violet staining. (C) Snail, Vimentin, N-cadherin, and E-cadherin expression were checked by Western blotting in HCT-116 and SW480 cells. **, P<0.01 or ***, P<0.001 *vs.* si-NC or OE-NC group. OE-NC, overexpression negative control; GOLPH3, Golgi phosphoprotein 3; GAPDH, glyceraldehyde-3-phosphate dehydrogenase; CRC, colorectal cancer.

displayed the opposite effect (*Figure 4E*).

GOLPH3 promoted the membrane translocation of SMO in CRC cells

To further clarify the molecular mechanism underlying *GOLPH3*'s effect in CRC, RNA-seq was performed in SW480 cells with knockdown of *GOLPH3*. The differentially expressed genes (DEGs) between si-NC and si-GOLPH3 groups are shown in in *Figure 5A*, while the upregulated and downregulated genes are shown in *Figure 5B*. Next, we conducted KEGG enrichment analysis on these DEGs and found that these DEGs were enriched in many pathways, including Hedgehog signaling pathway (*Figure 5C*,*5D*). Based on TCGA database, KEGG enrichment analysis was also conducted. The results revealed that Hedgehog signaling pathway and glycolysis were regulated by *GOLPH3* (*Figure 5E*,*5F*). A previous study indicated that SMO, a key protein in Hedgehog signaling pathway, could affect the glycolytic process in cells through regulating AMPK (21). In process of the infinite proliferation of cancer cells, glycolysis is a key pathological factor. Therefore, we speculated that SMO/AMPK pathway-mediated glycolysis might be the underlying

© AME Publishing Company.

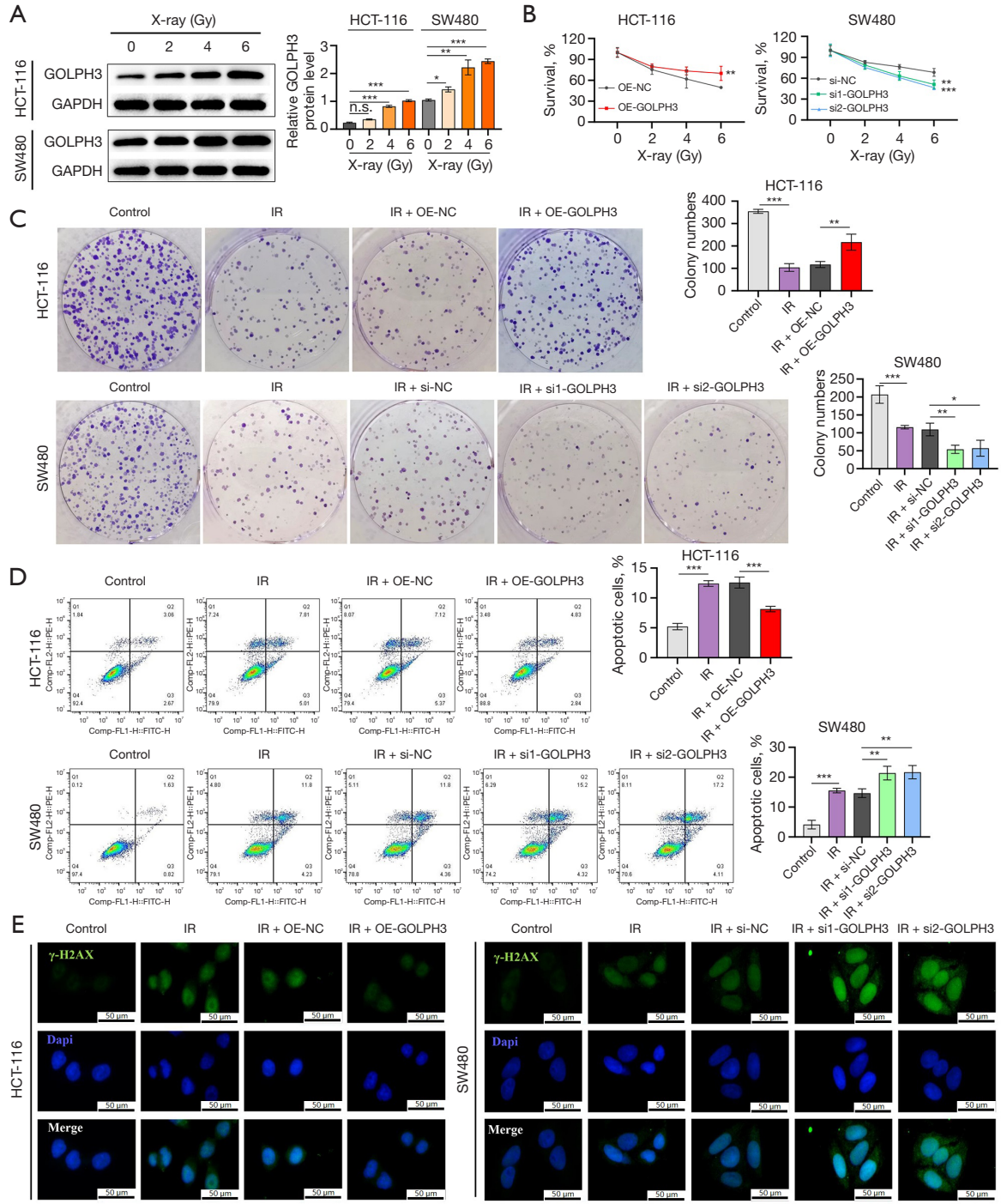

Figure 4 *GOLPH3* promoted the radiotherapy resistance of CRC cells by inhibiting DSBs. (A) GOLPH3 expression was assessed by Western blotting in HCT-116 and SW480 cells. (B) HCT-116 and SW480 cell viability were analyzed with CCK-8 assay. (C) Colony formation assay followed by crystal violet staining was performed for assessing HCT-116 and SW480 cell proliferation. (D) HCT-116 and SW480 cell apoptosis were analyzed with flow cytometry. (E) IF assay was used to assess γ-H2AX expression. *, P<0.05, **, P<0.01 or ***, P<0.001 *vs.* si-NC or OE-NC group; n.s., not significant. GOLPH3, Golgi phosphoprotein 3; GAPDH, glyceraldehyde-3-phosphate dehydrogenase; OE-NC, overexpression negative control; IR, ionizing radiation; CRC, colorectal cancer; CCK-8, Cell Counting Kit-8; IF, immunofluorescence.

© AME Publishing Company.

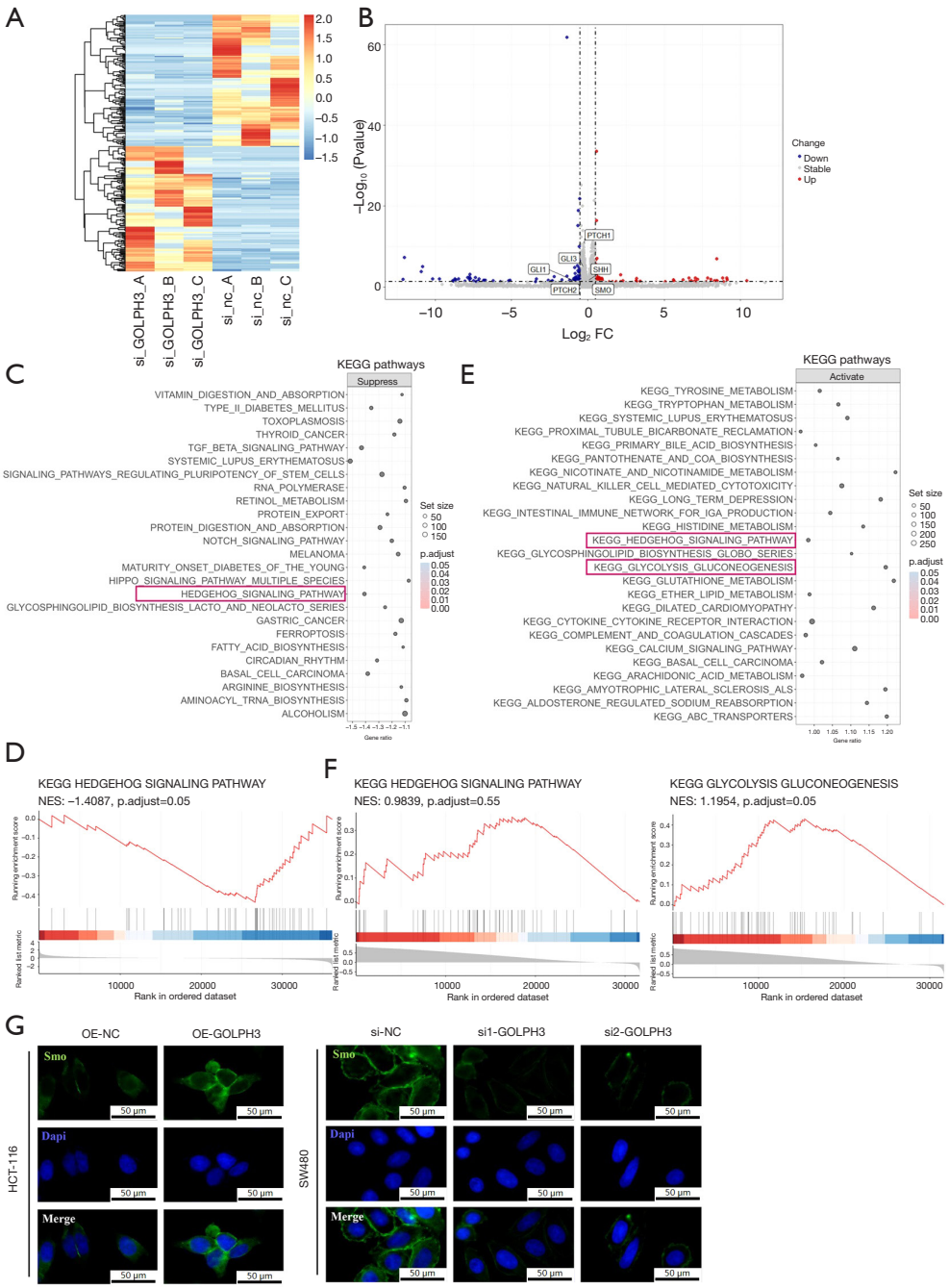

Figure 5 *GOLPH3* promoted the membrane translocation of SMO in CRC cells. (A) Heat map and (B) volcano plot of DEGs after RNA-seq between si-NC and si-GOLPH3 groups in SW480 cells. (C) The pathways in which DEGs were enriched according to RNA-seq were analyzed by KEGG enrichment analysis. (D) DEGs between the si-NC and si-GOLPH3 groups were enriched in Hedgehog signaling pathway. (E) Based on TCGA database, the pathways related to *GOLPH3* were analyzed using KEGG enrichment analysis. (F) Based on TCGA database, KEGG enrichment analysis indicated that *GOLPH3* could regulate Hedgehog signaling pathway and glycolysis. (G) SMO expression was detected by IF assay in HCT-116 and SW480 cells. GOLPH3, Golgi phosphoprotein 3; SMO, smoothened; FC, fold change; KEGG, Kyoto Encyclopedia of Genes and Genomes; CRC, colorectal cancer; DEGs, differentially expressed genes; RNA-seq, RNA sequencing; NC, negative control; TCGA, The Cancer Genome Atlas; NES, normalized enrichment score; OE-NC, overexpression negative control; IF, immunofluorescence.

© AME Publishing Company.

mechanism involved in the oncogenic effect of *GOLPH3*. *GOLPH3* is located on the Golgi apparatus and is mainly responsible for protein transport (22). SMO is mainly localized on the cell membrane. Through RNA-seq and TCGA analysis, we found that *GOLPH3* affected Hedgehog signaling pathway and glycolysis but exerted no significant effect on the expression of SMO protein (*Figure 5B*). Therefore, we speculated that *GOLPH3* might promote SMO's membrane translocation and enhance its activity. As expected, IF indicated that *GOLPH3* overexpression promoted the localization of SMO on the cell membrane, while *GOLPH3* knockdown inhibited the localization of SMO on the cell membrane (*Figure 5G*).

GOLPH3 promoted CRC cell glycolysis via activation of SMO/AMPK signaling

To verify our hypothesis that *GOLPH3* could regulate CRC cell glycolysis, we examined CRC cell metabolism. *GOLPH3* overexpression increased ECAR level and decreased OCR level in HCT-116 cells, while *GOLPH3* knockdown decreased ECAR level and increased OCR level in SW480 cells (*Figure 6A*). Moreover, *GOLPH3* overexpression enhanced glucose uptake and lactate production, while glucose uptake and lactate production were inhibited by *GOLPH3* knockdown (*Figure 6B*,*6C*). The results of Western blotting revealed that *GOLPH3* overexpression raised the levels of p-AMPK/AMPK, and PKM2, while *GOLPH3* knockdown led to the opposite (*Figure 6D*). In addition, we used SMO agonist (SAG) and AMPK agonist (GSK621) to treat SW480 cells with *GOLPH3* knockdown and found that the addition of SAG and GSK621 could reverse the inhibitory effect of *GOLPH3* knockdown on glucose uptake and lactate production (*Figure 6E*).

The lactate produced by CRC cells during glycolysis further increased GOLPH3 expression through H3K18la

An increasing number of studies have found that the glycolysis product lactate can cause protein lactylation modification, thereby affecting protein stability and expression (23-25), with H3K18la being the most intensely studied. Through Western blotting analysis, we found that H3K18la expression was increased in CRC tissues (*Figure 7A*), suggesting that H3K18 lactylation is common in CRC. Next, we sought to determine whether the lactylation of H3K18la affected GOLPH3 expression in HCT-116 and SW480 cells. We found that GOLPH3 expression increased with the increase in lactate concentration (*Figure 7B*). In contrast, glycolysis inhibitor (2DG) and LDHA inhibitor (oxamate) inhibited GOLPH3 expression in a concentration-dependent manner (*Figure 7C*,*7D*). Furthermore, oxamate inhibited H3K18la expression, but Nala (sodium lactate) reversed the inhibitory effect of oxamate on GOLPH3 and H3K18la expression (*Figure 7E*). In addition, the results of the ChIP and qPCR assay indicated that H3K18la was enriched on the *GOLPH3* promoter, but 2DG and oxamate reduced the enrichment of H3K18la in the *GOLPH3* promoter (*Figure 7F*,*7G*).

GOLPH3 knockdown inhibited the oncogenicity of CRC cells in vivo

To assess *GOLPH3*'s role *in vivo*, xenograft tumor experiments were conducted in mice. Mice in the sh-GOLPH3 group had smaller tumor volume and weight (*Figure 8A-8C*). Compared to the sh-NC condition, *GOLPH3* knockdown reduced the number of Ki-67-positive cells and increased the proportion of apoptotic cells in tumor tissues (*Figure 8D*). Additionally, *GOLPH3* knockdown decreased the abundance of SMO, PKM2, and H3K18la-positive cells in tumor tissues (*Figure 8E*,*8F*). Western blot analysis also confirmed that *GOLPH3* knockdown inhibited GOLPH3, p-AMPK, PKM2, and H3K18la expression in tumor tissues (*Figure 8G*,*8H*).

Discussion

CRC has emerged as a worldwide health concern due to its high mortality (26,27). Therefore, the mechanism of CRC pathogenesis and novel targets for CRC treatment urgently need to be defined. As a phosphatidylinositol 4-phosphate (PI4P) binding protein, GOLPH3 is required for the regulation of Golgi glycosylation, vesicle trafficking, Golgi ribbon structure maintenance, and mitochondrial cardiolipin production (28,29). Recent studies have demonstrated that *GOLPH3* expression is elevated in various cancers, such as BC, PDAC, prostate cancer, and glioma (15,16,30,31). In our study, we additionally found that *GOLPH3* expression was increased in CRC tissues and cells and that a high expression of *GOLPH3* was predictive of a poor prognosis. *In vitro* experiments suggested that *GOLPH3* overexpression promoted CRC cell proliferation, migration, and invasion but inhibited apoptosis, as evidenced by the increase in Bcl-2, Snail, N-cadherin, and Vimentin expression and the

© AME Publishing Company.

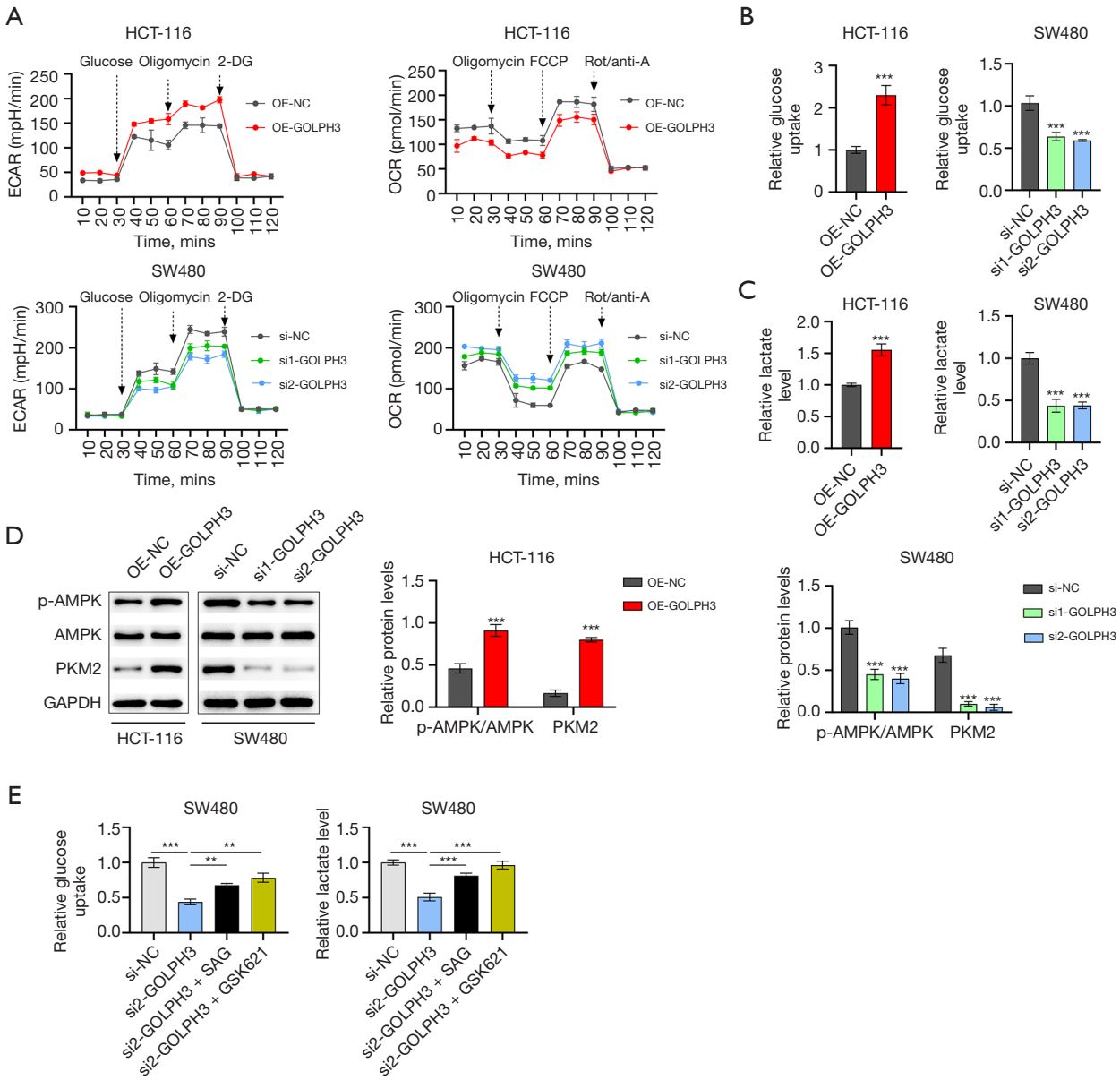

Figure 6 *GOLPH3* promoted CRC cell glycolysis via activation of SMO/AMPK signaling. (A) ECAR and OCR levels in HCT-116 and SW480 cells. (B) Glucose uptake in HCT-116 and SW480 cells. (C) Lactate level in HCT-116 and SW480 cells. (D) AMPK, p-AMPK, and PKM2 expression were checked by Western blotting in HCT-116 and SW480 cells. (E) Glucose uptake and lactate level in SW480 cells. **, P<0.01, ***, P<0.001 *vs.* si-NC or OE-NC group. GOLPH3, Golgi phosphoprotein 3; SMO, smoothened; AMPK, AMP-activated protein kinase; PKM2, pyruvate kinase M2; GAPDH, glyceraldehyde-3-phosphate dehydrogenase; CRC, colorectal cancer; ECAR, extracellular acidification rate; OCR, oxygen consumption rate; OE-NC, overexpression negative control; 2DG, 2-deoxyglucose; FCCP, carbonyl cyanide 4-(trifluoromethoxy) phenylhydrazone.

decrease in Bax, C-caspase-3, and E-cadherin expression. Meanwhile, *GOLPH3* knockdown reduced CRC cell proliferation, migration, and invasion but promoted apoptosis. Notably, *GOLPH3* knockdown suppressed tumor growth *in vivo*. These findings suggest that *GOLPH3* exerts carcinogenic effects within CRC.

In patients with locally advanced tumor, radiotherapy can provide effective tumor control (9,32). However,

© AME Publishing Company.

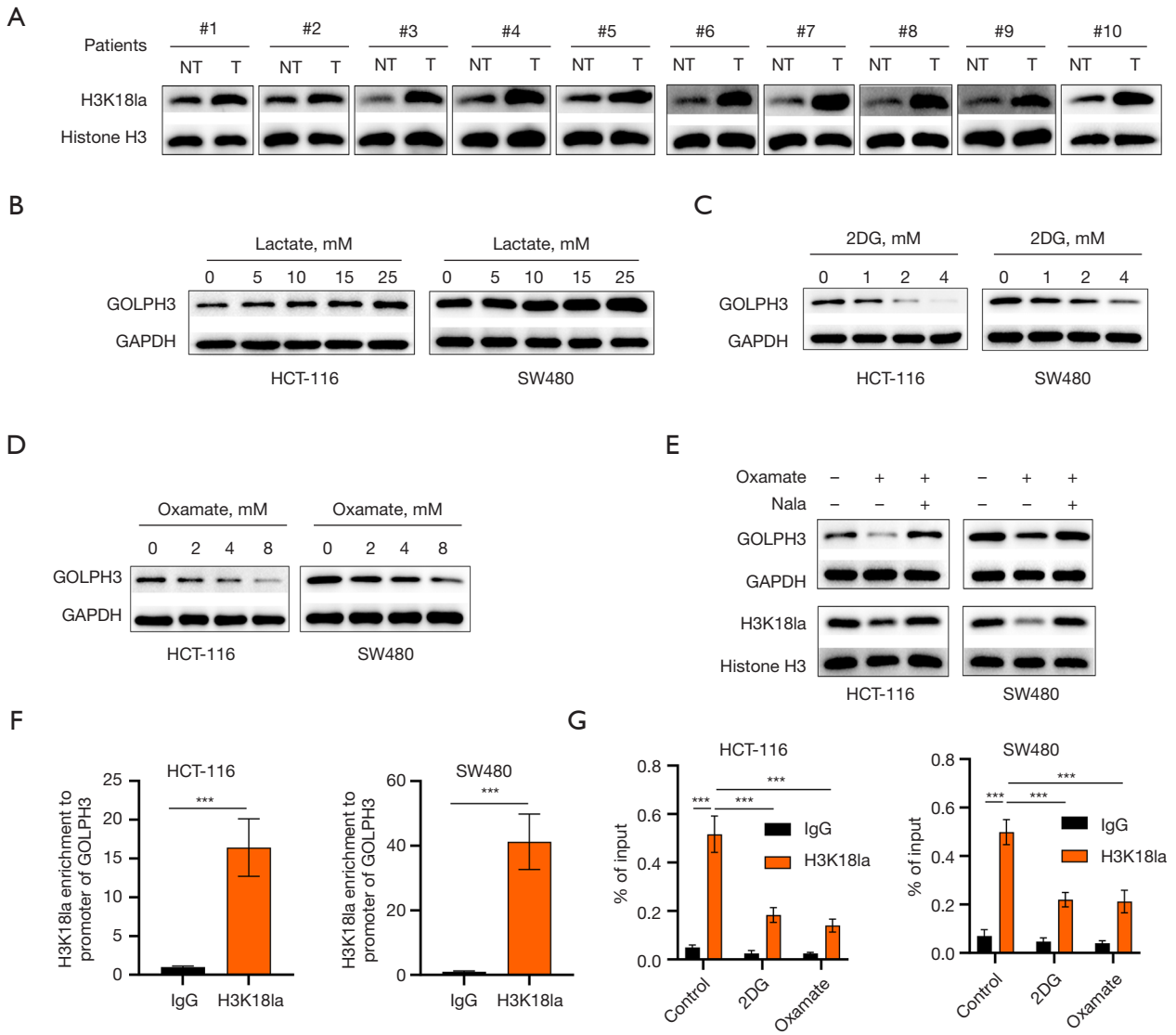

Figure 7 The lactate produced by CRC cells during glycolysis further increased GOLPH3 expression through H3K18la. (A) In CRC and normal tissues, H3K18la expression was checked using Western blotting. (B-D) GOLPH3 expression was assessed with Western blotting in HCT-116 and SW480 cells. (E) In HCT-116 and SW480 cells, GOLPH3 and H3K18la expression were assessed via Western blotting. (F,G) ChIP-qPCR assay was performed for detecting the enrichment of H3K18la on the *GOLPH3* promoter. ***, P<0.001 *vs.* IgG or H3K18la group. GOLPH3, Golgi phosphoprotein 3; H3K18la, H3 lysine 18 lactylation; NT, non-tumor; T, tumor; GAPDH, glyceraldehyde-3-phosphate dehydrogenase; IgG, immunoglobulin G; CRC, colorectal cancer; 2DG, 2-deoxyglucose; ChIP-qPCR, chromatin immunoprecipitation-quantitative polymerase chain reaction.

radioresistance response seriously threatens the quality of life of patients with CRC. In this study, we found that X-rays increased *GOLPH3* expression in CRC cells. Furthermore, under IR, *GOLPH3* overexpression promoted CRC cell proliferation and inhibited apoptosis, while *GOLPH3* knockdown produced the opposite result. These results indicate that *GOLPH3* enhances radiotherapy resistance in CRC cells. IR primarily eliminates tumor cells by inducing DNA damage, with DSBs being the most severe type of DNA damage (33). Tumor cells' sensitivity to radiation largely depends on their ability to recognize and respond to DSBs (34). In our study, *GOLPH3* overexpression decreased γ-H2AX (a sensitive DSB marker) expression under IR, while *GOLPH3* knockdown further increased γ-H2AX

© AME Publishing Company.

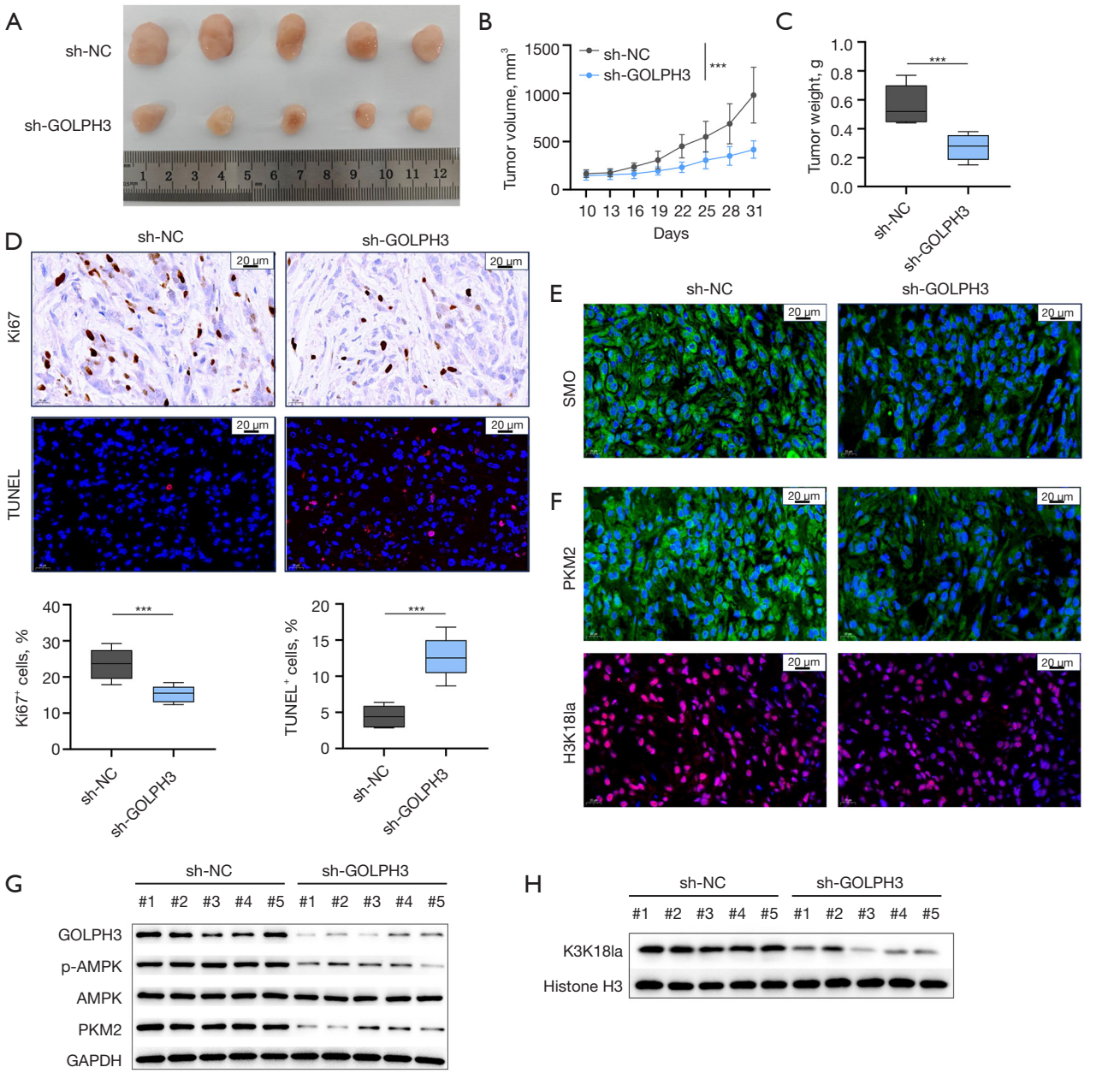

Figure 8 *GOLPH3* knockdown inhibited the oncogenicity of CRC cells *in vivo*. (A) Image of the xenograft tumor. The (B) volume and (C) weight of the xenograft tumor. (D) Ki-67 IHC staining and TUNEL staining on tumor tissues were performed by detecting tumor growth and cell death. (E) SMO expression in tumor tissues was detected through IF staining. (F) In tumor tissues, IF staining was employed for assessing PKM2 and H3K18la expression. (G) Western blotting was conducted to survey GOLPH3, p-AMPK, AMPK, and PKM2 expression in tumor tissues. (H) In tumor tissues, H3K18la expression was measured via Western blotting. ***, P<0.001 *vs.* sh-NC group. GOLPH3, Golgi phosphoprotein 3; H3K18la, H3 lysine 18 lactylation; SMO, smoothened; AMPK, AMP-activated protein kinase; PKM2, pyruvate kinase M2; NC, negative control; GAPDH, glyceraldehyde-3-phosphate dehydrogenase; CRC, colorectal cancer; IHC, immunohistochemistry; IF, immunofluorescence; TUNEL, terminal-deoxynucleoitidyl transferase mediated nick end labeling.

© AME Publishing Company.

expression. Taken together, these findings indicate that *GOLPH3* promotes CRC cells' radiotherapy resistance by inhibiting DSBs.

Metabolic reprogramming has been considered a hallmark of invasive cancer cells (35-37). Unlike normal cells, cancer cells prefer aerobic glycolysis even when oxygen is abundant (38). Glycolysis (also known as the Warburg effect) is characterized by a higher rate of glucose uptake and elevated production of adenosine triphosphate (ATP) and lactate, which promotes tumor progression (39,40). Recent studies have revealed that the inhibition of glycolysis represses CRC progression (41-43), which highlights the promising role of glycolysis as a target of therapy. In our study, KEGG enrichment analysis indicated that glycolysis could be regulated by *GOLPH3*. The *in vitro* experiments showed that *GOLPH3* overexpression decreased OCR and increased ECAR, glucose uptake, and lactate production, while the opposite was observed in CRC cells with *GOLPH3* knockdown. In addition, *GOLPH3* knockdown inhibited PKM2 expression in cells and tumor tissues. In short, *GOLPH3* promotes CRC progression through accelerating glycolysis.

To further clarify the complex mechanism underlying *GOLPH3*'s effect in CRC, we performed RNA-seq in CRC cells to identify the pathways affected by *GOLPH3*. Notably, the DEGs caused by *GOLPH3* knockdown displayed enrichment in Hedgehog signaling pathway. Meanwhile, based on TCGA database, KEGG enrichment analysis also identified that Hedgehog signaling pathway was regulated by *GOLPH3*. As an evolutionarily conserved pathway, Hedgehog signaling is central to cell proliferation and differentiation, tissue development, and organ formation (44). Numerous studies have confirmed that the abnormal activation of Hedgehog signaling is related to the progression of multiple cancers, such as BC, endometrial cancer, and CRC (45-47). In Hedgehog signaling, transmembrane protein SMO is a key signal transducer (48). In the development of novel antitumor drugs, SMO inhibitors have emerged as an area of intense research in recent years (49). Teperino *et al.* reported that SMO could affect the glycolysis process in cells through regulating AMPK (21). In our study, *GOLPH3* overexpression promoted the localization of SMO on the cell membrane and increased p-AMPK expression, while *GOLPH3* knockdown led to opposite results. In addition, SMO and AMPK agonists reversed the inhibitory effect of *GOLPH3* knockdown on glucose uptake and lactate production. In summary, we for the first time demonstrated that *GOLPH3* activated the glycolysis of CRC cells through SMO/AMPK signaling. Further experiments including treating GOLPH3 knockdown cells with SAG and GSK621 to explore the mechanisms underlying the radiotherapy resistance of CRC are required in the following. Moreover, the regulation between GOLPH3 and glycolysis might be complex and multiple other signaling are involved. In addition to SMO/AMPK signaling, other signaling pathways involved in should be investigated further.

As a byproduct of glycolysis, lactate triggers histone lysine lactylation, thereby stimulating gene transcription (50). Recent studies have reported that histone lactylation, especially H3K18la, is involved in oncogenesis, tumor progression, tumor cellular metabolism reprogramming, and tumor immune escape (51-54). In our study, H3K18la expression was found to be increased in CRC tissues, suggesting that H3K18 lactylation is common in CRC. Furthermore, GOLPH3 expression was elevated by lactate treatment but reduced by 2DG and oxamate. Furthermore, the addition of Nala reversed the inhibitory effect of oxamate on GOLPH3 and H3K18la expression. In addition, ChIP and qPCR assay confirmed that H3K18la was enriched in the *GOLPH3* promoter but that 2DG and oxamate partially reversed this effect. Overall, H3K18la mediated by lactate can be enriched on the *GOLPH3* promoter, thereby promoting GOLPH3 expression.

Conclusions

GOLPH3 was upregulated in CRC tissues, and low *GOLPH3* expression was predictive of a better prognosis. Moreover, *GOLPH3* knockdown inhibited malignant biological behaviors, reduced radiotherapy resistance, and impeded tumor growth in CRC. In terms of mechanism, *GOLPH3* activated AMPK mediated glycolysis by promoting the localization of SMO on the cell membrane; meanwhile, lactate, the final product of glycolysis could induce H3K18 lactylation, and H3K18la was enriched in *GOLPH3* the promoter, further increasing GOLPH3 expression (*Figure 9*). Our findings suggest that targeting the GOLPH3-SMO-AMPK axis has potential clinical value for CRC treatment. The feasibility of therapeutic strategies targeting GOLPH3 should be further validated in clinic.

© AME Publishing Company.

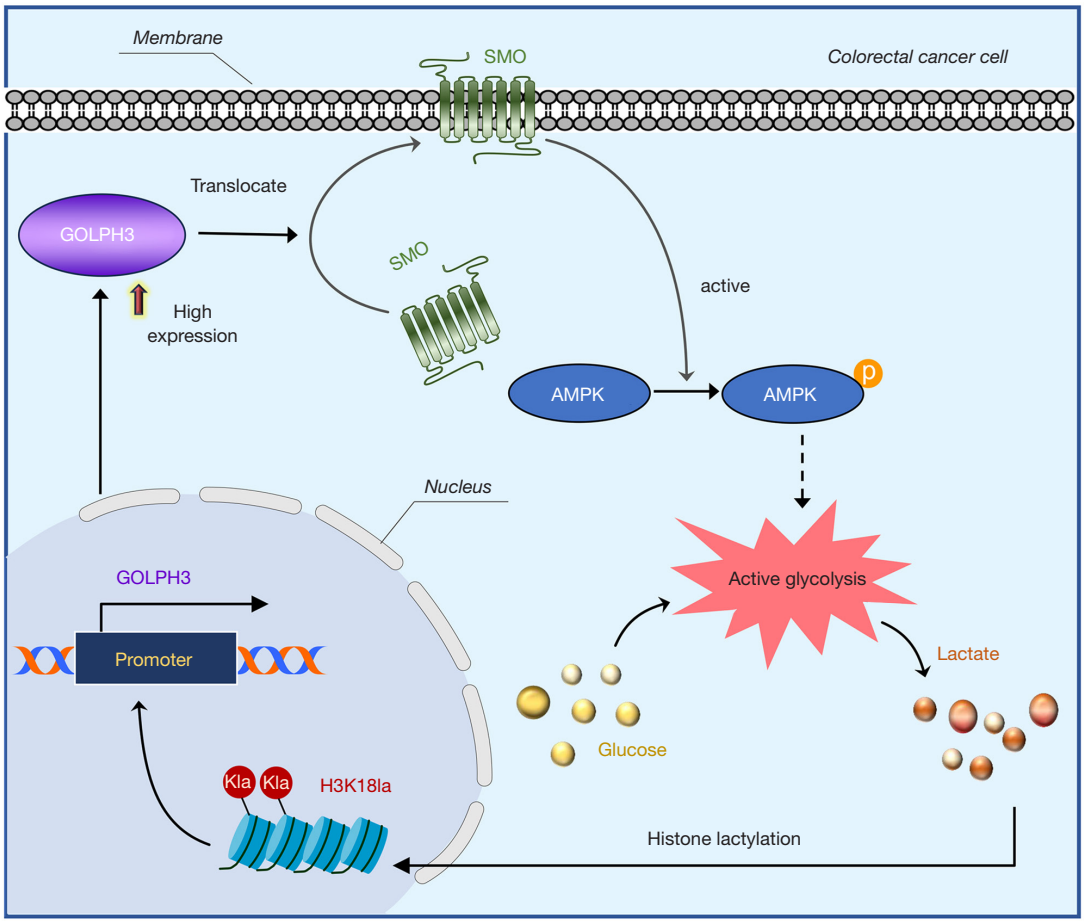

Figure 9 Schematic of the proposed mechanism by which the GOLPH3-SMO-AMPK axis promotes CRC progression. GOLPH3, Golgi phosphoprotein 3; SMO, smoothened; AMPK, AMP-activated protein kinase; H3K18la, H3 lysine 18 lactylation; CRC, colorectal cancer.

Acknowledgments

None.

Footnote

Reporting Checklist: The authors have completed the ARRIVE and MDAR reporting checklists. Available at https://jgo.amegroups.com/article/view/10.21037/jgo-2025-193/rc

Data Sharing Statement: Available at https://jgo.amegroups.com/article/view/10.21037/jgo-2025-193/dss

Peer Review File: Available at https://jgo.amegroups.com/article/view/10.21037/jgo-2025-193/prf

Funding: This research was funded by the Joint Fund for Tumor Prevention and Treatment of Shandong Natural Science Foundation (No. ZR2019LZL010 to K.Z.), the Joint Fund for Innovation and Development of Shandong Natural Science Foundation (No. ZR2023LZL006 to C.Z.), and the National Natural Science Foundation of China (No. 82303347 to Z.G.).

Conflicts of Interest: All authors have completed the ICMJE uniform disclosure form (available at https://jgo.amegroups.com/article/view/10.21037/jgo-2025-193/coif). K.Z. reports funding from the Joint Fund for Tumor Prevention and Treatment of Shandong Natural Science Foundation (No. ZR2019LZL010). C.Z. reports funding from the Joint Fund for Innovation and Development of Shandong Natural Science Foundation (No. ZR2023LZL006). Z.G. reports

© AME Publishing Company.

funding from the National Natural Science Foundation of China (No. 82303347). The other authors have no conflicts of interest to declare.

Ethical Statement: The authors are accountable for all aspects of the work in ensuring that questions related to the accuracy or integrity of any part of the work are appropriately investigated and resolved. This study was conducted in accordance with the Declaration of Helsinki and its subsequent amendments. The study was approved by the Ethics Committee of Shandong Cancer Hospital & Institute Affiliated to Shandong First Medical University (No. SDTHEC 2023006022) and informed consent was taken from all the patients. Animal experiments were performed under a project license (No. SDTHEC 2023006021) granted by the Animal Ethics Committee of Shandong Cancer Hospital & Institute Affiliated to Shandong First Medical University, in compliance with the guidelines of Shandong Cancer Hospital & Institute Affiliated to Shandong First Medical University for the care and use of animals.

Open Access Statement: This is an Open Access article distributed in accordance with the Creative Commons Attribution-NonCommercial-NoDerivs 4.0 International License (CC BY-NC-ND 4.0), which permits the non-commercial replication and distribution of the article with the strict proviso that no changes or edits are made and the original work is properly cited (including links to both the formal publication through the relevant DOI and the license). See: https://creativecommons.org/licenses/by-nc-nd/4.0/.

References

1. Siegel RL, Wagle NS, Cercek A, et al. Colorectal cancer statistics, 2023. CA Cancer J Clin 2023;73:233-54.
2. Li YJ, Wang X, Wu YJ, et al. Access to colorectal cancer screening in populations in China, 2020: A coverage-focused synthesis analysis. Int J Cancer 2024;155:558-68.
3. Zeng H, Zhong X, Liu W, et al. Predicting treatment failure in stage III colon cancer patients after radical surgery. Front Oncol 2024;14:1397468.
4. Tzeng CW, Aloia TA. Colorectal liver metastases. J Gastrointest Surg 2013;17:195-201; quiz p.201-2.
5. Maeda Y, Shinohara T, Nagatsu A, et al. Long-Term Outcomes of Conversion Hepatectomy for Initially Unresectable Colorectal Liver Metastases. Ann Surg Oncol 2016;23 Suppl 2:S242-8.
6. Maughan TS, Adams RA, Smith CG, et al. Addition of cetuximab to oxaliplatin-based first-line combination chemotherapy for treatment of advanced colorectal cancer: results of the randomised phase 3 MRC COIN trial. Lancet 2011;377:2103-14.
7. Smith HG, Nilsson PJ, Shogan BD, et al. Neoadjuvant treatment of colorectal cancer: comprehensive review. BJS Open 2024;8:zrae038.
8. Eng C, Yoshino T, Ruíz-García E, et al. Colorectal cancer. Lancet 2024;404:294-310.
9. Kagawa Y, Smith JJ, Fokas E, et al. Future direction of total neoadjuvant therapy for locally advanced rectal cancer. Nat Rev Gastroenterol Hepatol 2024;21:444-55.
10. Zhou Y, Shao Y, Hu W, et al. A novel long noncoding RNA SP100-AS1 induces radioresistance of colorectal cancer via sponging miR-622 and stabilizing ATG3. Cell Death Differ 2023;30:111-24.
11. Akhunzianov AA, Rozhina EV, Filina YV, et al. Resistance to Radiotherapy in Cancer. Diseases 2025;13:22.
12. Scott KL, Chin L. Signaling from the Golgi: mechanisms and models for Golgi phosphoprotein 3-mediated oncogenesis. Clin Cancer Res 2010;16:2229-34.
13. Scott KL, Kabbarah O, Liang MC, et al. GOLPH3 modulates mTOR signalling and rapamycin sensitivity in cancer. Nature 2009;459:1085-90.
14. Brauer BK, Chen Z, Beirow F, et al. GOLPH3 and GOLPH3L maintain Golgi localization of LYSET and a functional mannose 6-phosphate transport pathway. EMBO J 2024;43:6264-90.
15. Song Q, Chen Q, Wang Q, et al. ATF-3/miR-590/GOLPH3 signaling pathway regulates proliferation of breast cancer. BMC Cancer 2018;18:255.
16. Wang K, Jiang S, Huang A, et al. GOLPH3 Promotes Cancer Growth by Interacting With STIP1 and Regulating Telomerase Activity in Pancreatic Ductal Adenocarcinoma. Front Oncol 2020;10:575358.
17. Song JW, Zhu J, Wu XX, et al. GOLPH3/CKAP4 promotes metastasis and tumorigenicity by enhancing the secretion of exosomal WNT3A in non-small-cell lung cancer. Cell Death Dis 2021;12:976.
18. Chen G, Kong P, Yang M, et al. Golgi Phosphoprotein 3 Confers Radioresistance via Stabilizing EGFR in Lung Adenocarcinoma. Int J Radiat Oncol Biol Phys 2022;112:1216-28.
19. Gao Y, Yin Z, Qi Y, et al. Golgi phosphoprotein 3 promotes angiogenesis and sorafenib resistance in hepatocellular carcinoma via upregulating exosomal miR-494-3p. Cancer Cell Int 2022;22:35.

20. Yu T, An Q, Cao XL, et al. GOLPH3 inhibition reverses oxaliplatin resistance of colon cancer cells via suppression of PI3K/AKT/mTOR pathway. Life Sci 2020;260:118294.
21. Teperino R, Amann S, Bayer M, et al. Hedgehog partial agonism drives Warburg-like metabolism in muscle and brown fat. Cell 2012;151:414-26.
22. Li T, You H, Zhang J, et al. Study of GOLPH3: a potential stress-inducible protein from Golgi apparatus. Mol Neurobiol 2014;49:1449-59.
23. Wang S, Huang T, Wu Q, et al. Lactate reprograms glioblastoma immunity through CBX3-regulated histone lactylation. J Clin Invest 2024;134:e176851.
24. Zhang R, Li L, Yu J. Lactate-induced IGF1R protein lactylation promotes proliferation and metabolic reprogramming of lung cancer cells. Open Life Sci 2024;19:20220874.
25. Tang F, Xiao D, Li X, et al. The roles of lactate and the interplay with m(6)A modification in diseases. Cell Biol Toxicol 2024;40:107.
26. Santucci C, Mignozzi S, Malvezzi M, et al. European cancer mortality predictions for the year 2024 with focus on colorectal cancer. Ann Oncol 2024;35:308-16.
27. Knudsen MD, Wang K, Wang L, et al. Colorectal Cancer Incidence and Mortality After Negative Colonoscopy Screening Results. JAMA Oncol 2025;11:46-54.
28. Rizzo R, Parashuraman S, D'Angelo G, et al. GOLPH3 and oncogenesis: What is the molecular link? Tissue Cell 2017;49:170-4.
29. Sechi S, Frappaolo A, Karimpour-Ghahnavieh A, et al. Oncogenic Roles of GOLPH3 in the Physiopathology of Cancer. Int J Mol Sci 2020;21:933.
30. Kiełb P, Kaczorowski M, Kowalczyk K, et al. Comparative analysis of GOLPH3 expression in lymph node-positive prostate cancer: immunohistochemistry staining patterns and clinical significance. Front Oncol 2023;13:1265788.
31. Wu S, Fu J, Dong Y, et al. GOLPH3 promotes glioma progression via facilitating JAK2-STAT3 pathway activation. J Neurooncol 2018;139:269-79.
32. Fadlallah H, El Masri J, Fakhereddine H, et al. Colorectal cancer: Recent advances in management and treatment. World J Clin Oncol 2024;15:1136-56.
33. Fujii S, Fuchs RP. Accidental Encounter of Repair Intermediates in Alkylated DNA May Lead to Double-Strand Breaks in Resting Cells. Int J Mol Sci 2024;25:8192.
34. Ostoich PV. The Significance of the Response: Beyond the Mechanics of DNA Damage and Repair-Physiological, Genetic, and Systemic Aspects of Radiosensitivity in Higher Organisms. Int J Mol Sci 2024;26:257.
35. Gao T, Yang L, Zhang Y, et al. Cancer metabolic reprogramming and precision medicine-current perspective. Front Pharmacol 2024;15:1450441.
36. Mao Y, Xia Z, Xia W, et al. Metabolic reprogramming, sensing, and cancer therapy. Cell Rep 2024;43:115064.
37. Aden D, Sureka N, Zaheer S, et al. Metabolic Reprogramming in Cancer: Implications for Immunosuppressive Microenvironment. Immunology 2025;174:30-72.
38. Kooshan Z, Cárdenas-Piedra L, Clements J, et al. Glycolysis, the sweet appetite of the tumor microenvironment. Cancer Lett 2024;600:217156.
39. Barba I, Carrillo-Bosch L, Seoane J. Targeting the Warburg Effect in Cancer: Where Do We Stand? Int J Mol Sci 2024;25:3142.
40. Zhao J, Jin D, Huang M, et al. Glycolysis in the tumor microenvironment: a driver of cancer progression and a promising therapeutic target. Front Cell Dev Biol 2024;12:1416472.
41. Chen J, Duan S, Wang Y, et al. MYG1 drives glycolysis and colorectal cancer development through nuclear-mitochondrial collaboration. Nat Commun 2024;15:4969.
42. Liu H, Chen X, Wang P, et al. PRMT1-mediated PGK1 arginine methylation promotes colorectal cancer glycolysis and tumorigenesis. Cell Death Dis 2024;15:170.
43. Zhang Y, Li L, Chu F, et al. Itraconazole inhibits tumor growth via CEBPB-mediated glycolysis in colorectal cancer. Cancer Sci 2024;115:1154-69.
44. Ingham PW, McMahon AP. Hedgehog signaling in animal development: paradigms and principles. Genes Dev 2001;15:3059-87.
45. Liu R, Yu Y, Wang Q, et al. Interactions between hedgehog signaling pathway and the complex tumor microenvironment in breast cancer: current knowledge and therapeutic promises. Cell Commun Signal 2024;22:432.
46. Yang H, Ji Y, Liu D, et al. LLGL2 targets the Hedgehog signaling pathway to influence malignant progression of endometrial cancer. Cell Signal 2025;127:111553.
47. Chen J, Chen W, Li X, et al. CBC-1 as a Cynanbungeigenin C derivative inhibits the growth of colorectal cancer through targeting Hedgehog pathway component GLI 1. Steroids 2024;206:109421.
48. Ogden SK, Fei DL, Schilling NS, et al. G protein Galphai functions immediately downstream of Smoothened in Hedgehog signalling. Nature 2008;456:967-70.
49. Rimkus TK, Carpenter RL, Qasem S, et al. Targeting the Sonic Hedgehog Signaling Pathway: Review of Smoothened and GLI Inhibitors. Cancers (Basel)

© AME Publishing Company.

2016;8:22.
50. Zhang D, Tang Z, Huang H, et al. Metabolic regulation of gene expression by histone lactylation. Nature 2019;574:575-80.
51. Yu J, Chai P, Xie M, et al. Histone lactylation drives oncogenesis by facilitating m(6)A reader protein YTHDF2 expression in ocular melanoma. Genome Biol 2021;22:85.
52. Yang J, Luo L, Zhao C, et al. A Positive Feedback Loop between Inactive VHL-Triggered Histone Lactylation and PDGFRβ Signaling Drives Clear Cell Renal Cell Carcinoma Progression. Int J Biol Sci 2022;18:3470-83.
53. Yang Z, Yan C, Ma J, et al. Lactylome analysis suggests lactylation-dependent mechanisms of metabolic adaptation in hepatocellular carcinoma. Nat Metab 2023;5:61-79.
54. Xiong J, He J, Zhu J, et al. Lactylation-driven METTL3-mediated RNA m(6)A modification promotes immunosuppression of tumor-infiltrating myeloid cells. Mol Cell 2022;82:1660-1677.e10.

Cite this article as: Zhu K, Fan J, Cai H, Zhou C, Gong Z, Li Z, Yu J. The highly expressed *GOLPH3* in colorectal cancer cells activates smoothened to drive glycolysis and promote cancer cell growth and radiotherapy resistance. J Gastrointest Oncol 2025;16(2):415-434. doi: 10.21037/jgo-2025-193

© AME Publishing Company.